Molecular Layer-by-Layer Assembled Thin-Film Composite Membranes for Water Desalination

ARTICLE *in* ADVANCED MATERIALS · SEPTEMBER 2013

Impact Factor: 17.49 · DOI: 10.1002/adma.201302030 · Source: PubMed

11 AUTHORS, INCLUDING:

Christopher M Stafford
National Institute of Standards and Techno…
119 PUBLICATIONS **3,722** CITATIONS
SEE PROFILE

Edwin P Chan
National Institute of Standards and Techno…
39 PUBLICATIONS **1,010** CITATIONS
SEE PROFILE

Joona Bang
Korea University
105 PUBLICATIONS **2,454** CITATIONS
SEE PROFILE

COMMUNICATION

Molecular Layer-by-Layer Assembled Thin-Film Composite Membranes for Water Desalination

Joung-Eun Gu, Seunghye Lee, Christopher M. Stafford, Jong Suk Lee, Wansuk Choi, Bo-Young Kim, Kyung-Youl Baek, Edwin P. Chan, Jun Young Chung,* Joona Bang,* and Jung-Hyun Lee**

Growing concerns over access to clean and safe water have led to intense research on advanced materials for water purification.[1–4] To meet this challenge, seawater desalination and water treatment using reverse osmosis (RO) membranes have become one of the most energy-efficient technologies for creating sustainable water supplies. State-of-the-art commercial RO membranes utilize a thin film composite (TFC) design consisting of a highly crosslinked polyamide (PA) selective layer on a microporous polymeric support, wherein separation of water from solutes occurs through the dense PA layer.[5] The structural characteristics (e.g., chemistry, molecular topology, homogeneity) of the PA layer are thus critically important in controlling the permselectivity of the TFC membrane. The PA selective layer is traditionally fabricated via interfacial polymerization of *m*-phenylenediamine (MPD) and trimesoyl chloride (TMC), which results in the formation of a highly crosslinked, fully-aromatic PA network.[5,6] The rapid reaction rate between the diamine and triacid chloride leads to the system quickly reaching a gel point, wherein subsequent diffusion of both monomers becomes restricted.[7] Thus, interfacial polymerization produces selective layers that are highly depth-heterogeneous with limited control over film thickness and have ridge-and-valley structures, all of which confound our understanding of the membrane performance behavior and ultimately limit our ability to optimize permselectivity.

We recently reported on a process for generating PA layers on nonporous substrates that can overcome the limitations of traditional interfacial polymerization.[8,9] Termed molecular layer-by-layer (mLbL) deposition, this process involves the sequential reaction of a diamine and a triacid chloride to build chemically robust, highly crosslinked, and dense networks that do not suffer the kinetic and mass transfer limitations of traditional interfacial polymerization. Consequently, mLbL represents a platform for creating selective layers whose thickness, topology, and local chemical composition are controllable at monomer length-scales that are not achievable via interfacial polymerization. Specifically, the thickness of the selective layer can be controlled by the number of deposition cycles while its topology and local chemical composition can be controlled by the type and sequence of monomers used in the mLbL assembly. Since this process assembles monomers at the molecular scale, the resulting layers are relatively smooth compared to their interfacially polymerized counterparts.[9] Furthermore, unlike interfacial polymerization that requires the formation of a reaction interface between an aqueous and an organic solution, mLbL is not limited to specific solvents, thus broadening the types of chemistries that can be integrated into the selective layer.[10–12]

Despite its promising potential, translating the mLbL assembly to actual membranes for practical applications has remained challenging. The main hurdle lies in creating a defect-free mLbL layer on a porous support (akin to the TFC design) while avoiding deposition of monomers within the support itself. Such an assembly has recently been attempted by Qian et al., who sequentially deposited a tetrafunctional amine and a tetrafunctional acid chloride on a microporous ultrafiltration support.[13] Although such membranes were shown to be highly selective for multivalent ions, they exhibited a relatively low rejection ($R \approx 46\%$) of monovalent salts such as NaCl, likely due to the large monomer size and associated increase in fractional free volume of the resultant selective layer network. Moreover, monomer deposition inside the porous support possibly prevented the formation of defect-free layers, which deteriorated selectivity. As a result, the performance is far below the requirements for seawater desalination via reverse osmosis.

Here, we report on the successful design, construction, and performance of mLbL membranes and demonstrate that these materials exceed the performance of membranes synthesized through conventional interfacial polymerization. The critical step in realizing the mLbL membranes is that we apply

J.-E. Gu, W. Choi, B.-Y. Kim, Dr. K.-Y. Baek, Dr. J.-H. Lee
Center for Materials Architecturing
Korea Institute of Science and Technology (KIST)
Seoul 136-791, Korea
E-mail: leejhy@kist.re.kr
S. Lee, W. Choi, Prof. J. Bang
Department of Chemical and Biological Engineering
Korea University
Seoul 136-713, Korea
E-mail: joona@korea.ac.kr
Dr. C. M. Stafford, Dr. E. P. Chan
Materials Science and Engineering Division
National Institute of Standards and Technology (NIST)
Gaithersburg, Maryland 20899, USA
E-mail: edwin.chan@nist.gov
Dr. J. S. Lee
Green City Technology Institute
Korea Institute of Science and Technology (KIST)
Seoul 136-791, Korea
Dr. J. Y. Chung
School of Engineering and Applied Sciences
Harvard University
Cambridge, Massachusetts 02138, USA
E-mail: jchung@seas.harvard.edu

DOI: 10.1002/adma.201302030

an ultrathin interlayer atop the porous support to prevent the penetration of reactive monomer solutions into the support. We then conduct mLbL assembly using traditional monomers in RO membrane fabrication (i.e., TMC and MPD), which are rigid aromatic monomers that display relatively low fractional free volume upon network formation. The mLbL process produced highly selective PA layers with precisely-controlled thickness, minimal surface roughness, and well-defined chemical composition. As a result, only 15 cycles of mLbL assembly were needed to achieve the targeted NaCl rejection (R > 98%) while the flux was about 75% greater than a traditional interfacially polymerized PA membrane. The high salt rejection demonstrates that the structure of the mLbL selective layer is sufficiently similar to traditional interfacial polymerization, while the reduced thickness of the selective layer (≈25 nm) equates to a reduced hydraulic resistance and shorter diffusive path length for water to pass through the membrane. Additionally, we show that the reduced surface roughness and chemical homogeneity achieved by mLbL mitigated membrane fouling.

A schematic comparison of the mLbL-assembled and interfacially polymerized (IP) PA-TFC membranes is shown in **Figure 1**. We start with a poly(acrylonitrile) (PAN) ultrafiltration support with an average pore diameter of 15 nm. To block the pore structure of the PAN support, we coat the support with an interlayer consisting of one bilayer of polyelectrolyte layer-by-layer (LbL) assembly of branched-poly(ethyleneimine) (PEI, positively charged) and poly(acrylic acid) (PAA, negatively charged) through electrostatic interaction. The PAN support is hydrolyzed with NaOH prior to adsorption of PEI to generate the requisite net negative charge on the surface. We investigated other interlayers (e.g., interfacially polymerized semi-aromatic PA layer using TMC and piperazine, poly(allylamine)/PAA bilayer, branched-PEI layer) and found that a combination of high molecular mass, branched-PEI and PAA provided the most efficient coating for the porous support with the minimal flux loss, as evidenced by the disappearance of pores under scanning electron microscopy (SEM, See Supporting Information Figure S1). Additionally, the high density of carboxylic acid groups in PAA facilitates hydrogen bonding with the MPD monomer in the first mLbL deposition. The modified PAN support was then alternatively dipped into the two monomer solutions (MPD and TMC) in toluene and subsequently rinsed with proper solvents after each dipping step, leading to multilayered, crosslinked, fully-aromatic PA layers. Acetone and toluene were employed as rinsing solvents for MPD and TMC, respectively. The type of rinsing solvents for MPD plays an important role in the structures and properties of the mLbL layers.[8] We found that rinsing with acetone after the MPD deposition step resulted in markedly better membrane performance than other solvents (e.g., toluene, tetrahydrofuran, alcohols). We believe this is a result of the excellent solubility of MPD in acetone, the high volatility of acetone, and the relatively low swelling of the PAN support by acetone. The mLbL process was repeated until the desired PA thickness was reached, and reaction was terminated with the TMC deposition step to yield analogous surface chemistry and charge to those of interfacially polymerized PAs. The mLbL-assembled membranes are denoted as mLbL$_x$, where x is the number of deposition cycles. Note that mLbL$_0$ corresponds to the interlayer (PEI/PAA)-coated PAN membrane with no mLbL deposition. As a control, we also performed traditional interfacial polymerization of MPD/TMC on the PAN support for comparison against our mLbL membranes (see Supporting Information for details). Chemical analysis by Fourier transform-infrared spectroscopy (FT-IR) and X-ray photoelectron spectroscopy (XPS) revealed that both mLbL-PA and IP-PA have similar chemical structures (See Supporting Information Figure S2).

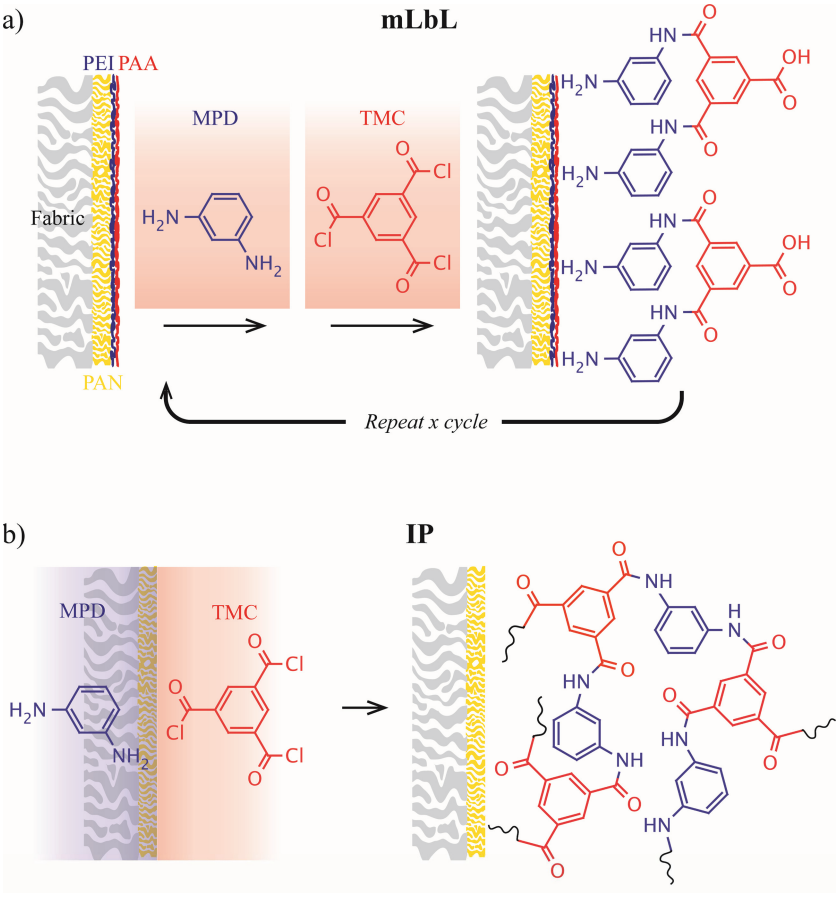

Figure 1. Schematic illustration of the fabrication of polyamide thin film composite membranes via (a) molecular layer-by-layer (mLbL) deposition and (b) traditional interfacial polymerization (IP).

Next, we evaluated the performance of the mLbL-PA membranes via crossflow filtration and compared those results to the IP-PA membrane (control). The water flux (J_w) and salt rejection (R) of mLbL-PA membranes were measured as a function of the deposition cycle number (**Figure 2**a). The results

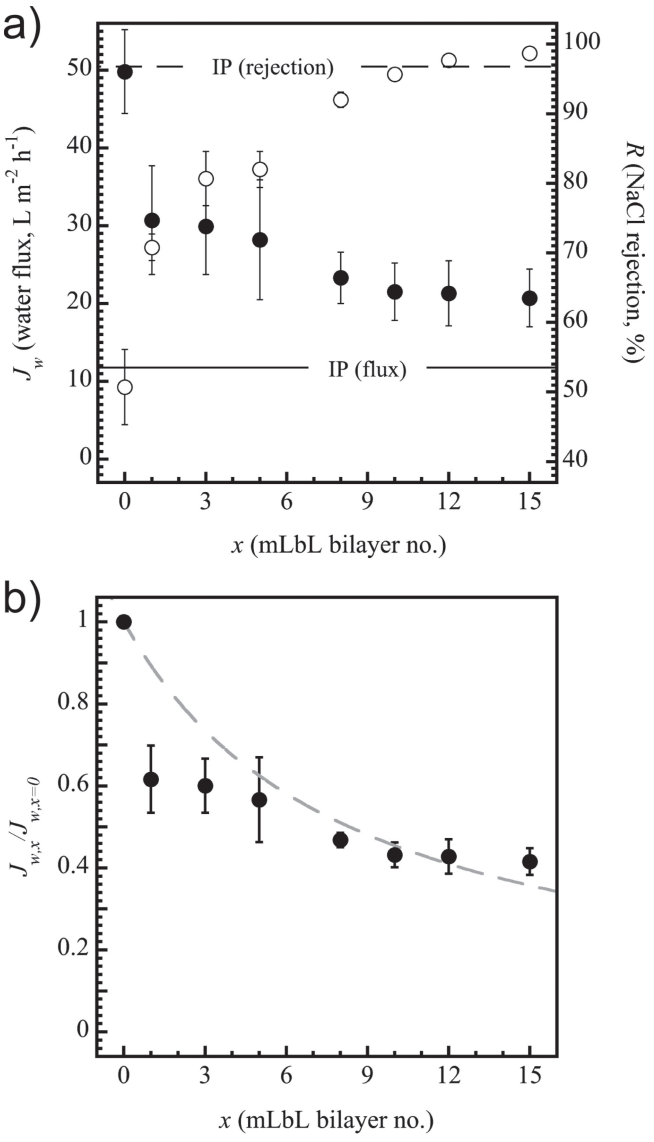

Figure 2. (a) Water flux (J_w, filled symbols) and NaCl rejection (R, unfilled symbols) of mLbL-assembled polyamide (PA) membranes as a function of the deposition cycle number (x). The horizontal solid and dashed lines denote the water flux and NaCl rejection values of the interfacially polymerized (IP) PA membrane, respectively. (b) Normalized water flux of mLbL-assembled PA membranes as a function of deposition cycle number (x). The measured water flux was normalized by the water flux of PEI/PAA-coated PAN (0 cycle of mLbL). The dashed line is a fit of the data to Equation (3), which is a resistance-in-series model comprised of the multiple discrete layers of the composite membrane. All performance tests were conducted using aqueous solution of NaCl (2,000 mg L^{-1}) at an operating pressure of 15.5 bar.

show that membrane performance was tuned by adjusting the number of mLbL bilayers. In particular, the $mLbL_{10}$ exhibited an ≈82% increase in water flux [(21.5 ± 3.7 *vs.* 11.8 ± 3.3) L m^{-2} h^{-1}] with similar rejection [(95.7 ± 0.9 *vs.* 96.8 ± 0.9)%] compared with the interfacially polymerized analog. More importantly, as the number of deposition cycles increased, rejection increased progressively until it reached (98.7 ± 0.3)% for the $mLbL_{15}$, which was even higher than that of the IP-PA membrane, (96.8 ± 0.9)%, while still exhibiting a remarkable 75% enhancement in water flux, (20.7 ± 3.7) L m^{-2} h^{-1}. This demonstrates that mLbL deposition can create defect-free, highly-selective layers on porous supports in a controlled manner that can be used for RO membranes. Practically, it would be desirable to compare the performance of the mLbL membrane to commercial ones, although it is a difficult comparison because commercial membranes are typically fabricated on polysulfone-based supports with highly-optimized performance using proprietary additives or treatments. Compared with a commercial RO membrane, the $mLbL_{15}$ exhibited comparable water flux with a slightly lower salt rejection than a commercial RO (SWC4+, Hydranautics, flux = (20.4 ± 0.5) L m^{-2} h^{-1} and R = (99.4 ± 0.1)%). However, we expect that the performance of the mLbL-assembled membrane can be significantly improved with optimization and modification akin to commercial membranes.

To better understand the performance of our mLbL membranes, we consider the solution diffusion model for transport through the membrane. According to the model, water flux (J_w) is dependent on the selective layer thickness (h), molecular mass of water (m_w), and its water permeability (P_w = product of water diffusivity and solubility), as well as the driving force (Δp) needed to overcome the osmotic pressure ($\Delta\pi$), normalized by thermal energy (RT). Because the thickness and water permeability are difficult to measure for actual membranes, these constants are substituted by a proportionality constant A, which is commonly referred to as the *apparent* water permeability coefficient.[6,14]

$$J_w = \frac{P_w}{h}\frac{m_w}{RT}(\Delta p - \Delta\pi) = A(\Delta p - \Delta\pi) \quad (1)$$

According to this equation, the water flux is inversely proportional to the selective layer thickness and directly proportional to the water permeability. Therefore, the reduced flux or increased hydraulic resistance (A^{-1}) after the first mLbL deposition can be attributed to the decreased water permeability as a result of the formation of a dense PA layer. The increase in the selective layer thickness with subsequent mLbL depositions leads to a progressive decrease in flux, which is again consistent with Equation (1), and can be described by a hydraulic resistance-in-series model:

$$J_{w,x} = \frac{(\Delta p - \Delta\pi)}{(A_{mLbL}^{-1} + A_{LbL}^{-1} + A_{PAN}^{-1})} \approx \frac{(\Delta p - \Delta\pi)}{(A_{mLbL}^{-1} + A_{LbL}^{-1})} \quad (2)$$

where A_{mLbL}, A_{LbL}, and A_{PAN} correspond to the apparent water permeability coefficient of the mLbL layer, the (PEI/PAA) LbL interlayer, and the PAN support, respectively. Because the porous PAN support has minimal hydraulic resistance relative to the dense mLbL layer and interlayer, the total water flux is determined primarily by A_{mLbL} and A_{LbL}. Comparing Equation (2) with the water flux for the composite membrane without mLbL ($J_{w,0}$), a normalized water flux scaling relationship is developed to demonstrate the contribution of the mLbL layer to the reduction in water flux.

$$\frac{J_{w,x}}{J_{w,0}} = \frac{A_{mLbL}}{(A_{mLbL} + A_{LbL})} = \left(1 + \frac{P_{LbL}}{P_{mLbL}}\frac{h_{mLbL}}{h_{LbL}}\right)^{-1} \quad (3)$$

We normalize the water flux of the $mLbL_x$ composite membrane with that of the composite membrane without mLbL as

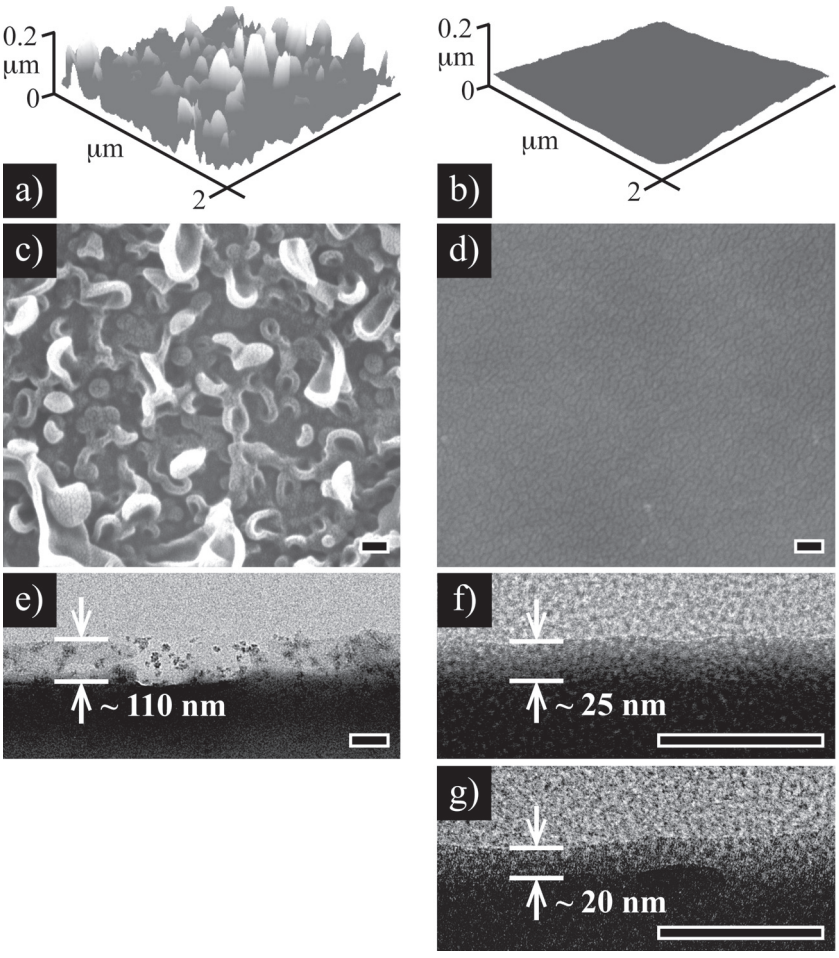

Figure 3. AFM height images of (a) the interfacially polymerized (IP) polyamide (PA) (*rms* ≈45.1 nm) and (b) the $mLbL_{15}$-assembled PA (*rms* ≈3.4 nm) membranes. Top-down SEM images of (c) the IP-PA and (d) the $mLbL_{15}$-PA membranes. Cross-sectional TEM images of the selective layers of (e) the IP-PA, (f) the $mLbL_{15}$-PA, and (g) the $mLbL_{10}$-PA membranes. Scale bar = 100 nm for all SEM and TEM images.

a function of x. Figure 2b displays the normalized water flux results along with the fit using Equation (3). Atomic force microscopy (AFM), SEM, and transmission electron microscopy (TEM) were used to characterize the morphology and thickness of the selective layers (**Figure 3**). AFM estimated the root mean square (*rms*) roughness of the IP-PA to be (45.1 ± 10.7) nm (Figure 3a) compared to (3.4 ± 0.6) nm for the $mLbL_{15}$-PA (Figure 3b). The top-down SEM images showed that the IP-PA exhibited the rough ridge-and-valley morphology that is typical of interfacially polymerized, fully-aromatic PAs (Figure 3c),[5,6] whereas the $mLbL_{15}$-PA had a significantly smoother surface (Figure 3d). Such a high level of roughness for the IP-PA has been attributed to the rapid, uncontrolled reaction rate occurring at multiple interfaces,[7,15] whereas the smoother surface for the mLbL-PA results from the controlled polymerization at a single monomer layer due to the stoichiometry-limiting feature of the mLbL approach.[9,11] The cross-sectional TEM images revealed the depth-heterogeneous nature of the IP-PA (Figure 3e), in contrast to the fairly dense and nearly depth-homogeneous structure of the mLbL-PA (Figures 3f and 3g). The selective layer thickness of the $mLbL_{15}$-PA membrane was determined to be ≈25 nm (see Supporting Information Figure S3), which is much thinner than that of the IP-PA layer (≈110 nm). Considering the selective layer thicknesses of the $mLbL_{10}$ and $mLbL_{15}$ membranes were 20 nm and 25 nm, respectively, the average thickness per mLbL deposition cycle can be calculated to be ≈1 nm. This is in good agreement with the result reported by Johnson *et al.*, who experimentally determined the linear film growth rate of ≈0.9 nm/cycle for mLbL deposition of TMC/MPD on silicon surfaces.[9] Using h_{LbL} = 10 nm and h_{mLbL} = (1 nm/cycle) × (cycle, x), the fit of Equation (3) to the data in Figure 2b calculates that the ratio of the water permeabilities, P_{LbL}/P_{mLbL} = 1.2. While pressure-dependent flux measurements are needed to quantify the water permeabilites of the selective layers, this permeability ratio value suggests that the mLbL layer is less permeable than the LbL interlayer, which is consistent with the notion that the mLbL is a denser selective layer that significantly reduces water and salt permeabilities. The non-ideal fit of Equation (3) to the data at lower x is likely due to non-linear growth of the mLbL on PEI/PAA-coated PAN for low cycle numbers. This deviation at lower x can also be attributed to the variation in the water permeability of the mLbL-PA for low cycle numbers, as evidenced by the deposition cycle-dependent wettability (see Supporting Information Figure S4).

Importantly, these results demonstrate that mLbL overrides the materials requirements imposed by Equation (1). Unlike the IP-PA membranes, whose thickness control and monomer chemistries are intimately coupled, mLbL offers a unique strategy for precise control of the selective layer thickness that is independent of the specific monomer chemistries. Because the thickness control is on the order of ≈1 nm per cycle, the mLbL-PA membranes can be tailored to have specific and enhanced water permeation rates compared to the IP-PA membrane while maintaining the improved salt rejection, as demonstrated by the $mLbL_{15}$.

The stability of the interlayer is a major concern for real world membrane operation. We confirmed that the mLbL-assembled membranes maintain performances without showing any structural destruction such as delamination after they are treated by aqueous solution of a moderate range of pH (3 to 10) for 2 h. We are currently investigating the stability of the mLbL membrane under various harsh conditions (e.g., extreme pHs or organic solvents).

Besides confirming that we have successfully fabricated the mLbL-PA atop the PAN porous supports, the microscopy images highlight the advantage of mLbL in creating more uniform and thinner skin layer with much smoother surface

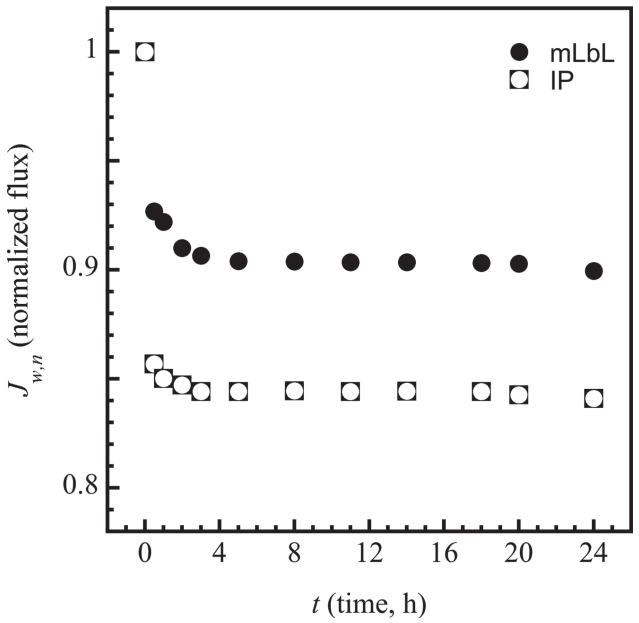

Figure 4. Fouling studies of the interfacially polymerized (IP) polyamide (PA) and the $mLbL_{15}$-assembled PA membranes. Water flux was normalized by the initial flux value as a function of filtration time upon the addition of BSA foulants (100 mg L^{-1}). The initial flux values were 13.2 L m^{-2} h^{-1} and 20.8 L m^{-2} h^{-1} for the IP-PA and the $mLbL_{15}$-PA membranes, respectively.

compared to traditional interfacial polymerization, despite the fact that the same monomers were used. In this case, the surface roughness of these membranes would greatly influence the fouling behavior.[16] To illustrate this aspect, the relative water fluxes of the $mLbL_{15}$-PA and IP-PA membranes were monitored as a function of time during the filtration with the feed solution containing a model foulant, bovine serum albumin (BSA). For both membranes, the flux decreased rapidly in the early stage until reaching a plateau. However, the mLbL-PA membrane exhibited a lower ultimate flux decline (≈10%) than the IP-PA membrane (≈16%), demonstrating its superior antifouling ability (**Figure 4**). The membrane surface charge is one of important properties governing the fouling, in particular for negatively charged BSA in the feed solution at pH > 4.8.[17] It was found that there was no discernible difference in zeta potential values at pH = 5.8 between $mLbL_{15}$-PA [(-22.4 ± 2.3) mV] and IP-PA [(-21.8 ± 1.9) mV] membranes within measurement error. Hence, the lower fouling propensity for the mLbL membrane is likely due to the surface smoothening combined with an observed enhancement in wettability (see Supporting Information Figure S4) imparted by mLbL deposition that can reduce the hydrophobic interaction between the hydrophobic BSA molecule and the membrane surface.[16,17]

In summary, we describe a new approach to fabricate highly permeable, low-fouling RO membranes via mLbL that enables the rational design of PA selective layers. The key attribute of mLbL is that it provides a straightforward means to control selective layer thickness, roughness, and chemical composition at the molecular level, which are characteristics critical to membrane performance. While optimization will provide further enhancement, our results show for the first time that mLbL enables the creation of ultrathin, defect-free selective layer with minimal roughness, achieving improved permselectivity and enhanced antifouling compared to traditional interfacially polymerized membranes. Additionally, the structure and function of the fabricated multilayered membrane could be further varied through changing monomer chemistry and incorporating functional nanomaterials. The versatility of this mLbL approach potentially offers a new pathway in the design of a wide range of nanoscale assemblies applicable to gas separation membranes, fuel cells, microfluidics, biomedical devices, and antifouling coatings.

Experimental Section

A detailed description of experimental materials and methods is provided in the Supporting Information.

Supporting Information

Supporting Information is available from the Wiley Online Library or from the author.

Acknowledgements

This work was supported by the KIST Institutional Programs (Project No. 2E23900, 2E23430, 2E23952) and partially supported by the Industrial Strategic Technology Development Program (10035373) funded by the Ministry of Knowledge Economy, Republic of Korea. S.L and J.B. acknowledge the support by the Korean Government (MOEHRD) (2012-014473), and also by the Human Resources Development Program of KETEP grant (No. 20114010203050). Official contribution of the National Institute of Standards and Technology.

Received: May 6, 2013
Revised: May 11, 2013
Published online: July 12, 2013

[1] D. L. Gin, R. D. Noble, *Science* **2011**, *332*, 674–676.
[2] M. Henmi, K. Nakatsuji, T. Ichikawa, H. Tomioka, T. Sakamoto, M. Yoshio, T. Kato, *Adv. Mater.* **2012**, *24*, 2238–2241.
[3] M. H. Park, C. Subramani, S. Rana, V. M. Rotello, *Adv. Mater.* **2012**, *24*, 5862–5866.
[4] X. S. Peng, J. Jin, Y. Nakamura, T. Ohno, I. Ichinose, *Nat. Nanotechnol.* **2009**, *4*, 353–357.
[5] M. Elimelech, W. A. Phillip, *Science* **2011**, *333*, 712–717.
[6] G. M. Geise, H. S. Lee, D. J. Miller, B. D. Freeman, J. E. McGrath, D. R. Paul, *J. Polym. Sci., Part B: Polym. Phys.* **2010**, *48*, 1685–1718.
[7] V. Freger, *Langmuir* **2003**, *19*, 4791–4797.
[8] E. P. Chan, J. H. Lee, J. Y. Chung, C. M. Stafford, *Rev. Sci. Instrum.* **2012**, *83*, 114102.
[9] P. M. Johnson, J. Yoon, J. Y. Kelly, J. A. Howarter, C. M. Stafford, *J. Polym. Sci., Part B: Polym. Phys.* **2012**, *50*, 168–173.
[10] A. H. Broderick, U. Manna, D. M. Lynn, *Chem. Mater.* **2012**, *24*, 1786–1795.
[11] N. Lomadze, M. Perez, O. Prucker, J. Ruhe, H. Reinecke, *Macromolecules* **2010**, *43*, 9056–9062.
[12] Z. Steiner, J. Miao, R. Kasher, *Chem. Commun.* **2011**, *47*, 2384–2386.
[13] H. D. Qian, S. H. Li, J. F. Zheng, S. B. Zhang, *Langmuir* **2012**, *28*, 17803–17810.
[14] A. K. Ghosh, B. H. Jeong, X. F. Huang, E. M. V. Hoek, *J. Membr. Sci.* **2008**, *311*, 34–45.
[15] V. Freger, *Langmuir* **2005**, *21*, 1884–1894.
[16] E. M. Vrijenhoek, S. Hong, M. Elimelech, *J. Membr. Sci.* **2001**, *188*, 115–128.
[17] T. Ishigami, K. Amano, A. Fujii, Y. Ohmukai, E. Kamio, T. Maruyama, H. Matsuyama, *Sep. Purif. Technol.* **2012**, *99*, 1–7.